

Third-order Hall effect in the surface states of a topological insulator

Tanay Nag,¹ Sanjib Kumar Das^{2,3}, Chuanchang Zeng^{4,5,*} and Snehasish Nandy^{6,7,†}

¹*Department of Physics and Astronomy, Uppsala University, Box 516, 75120 Uppsala, Sweden*

²*Department of Physics, Lehigh University, Bethlehem, Pennsylvania 18015, USA*

³*Leibniz Institute for Solid State and Materials Research (IFW) Dresden, Helmholtzstrasse 20, 01069 Dresden, Germany*

⁴*Centre for Quantum Physics, Key Laboratory of Advanced Optoelectronic Quantum Architecture and Measurement (MOE),*

School of Physics, Beijing Institute of Technology, Beijing 100081, China

⁵*Beijing Key Lab of Nanophotonics & Ultrafine Optoelectronic Systems,*

School of Physics, Beijing Institute of Technology, Beijing 100081, China

⁶*Theoretical Division, Los Alamos National Laboratory, Los Alamos, New Mexico 87545, USA*

⁷*Center for Nonlinear Studies, Los Alamos National Laboratory, Los Alamos, New Mexico 87545, USA*



(Received 11 October 2022; revised 6 April 2023; accepted 20 June 2023; published 28 June 2023)

Time reversal and inversion symmetric materials fail to yield linear and nonlinear responses since they possess net zero Berry curvature. However, higher-order Hall response can be generated in these systems upon constraining the crystalline symmetries. Motivated by the recently discovered third-order Hall (TOH) response mediated by Berry connection polarizability, namely, the variation of the Berry connection with respect to an applied electric field, here, we investigate the existence of such a Hall effect in the surface states of hexagonal warped topological insulators (e.g., Bi_2Te_3) under the application of only electric field. Using the semiclassical Boltzmann formalism, we investigate the effect of tilt and hexagonal warping on the Berry connection polarizability tensor and, consequently, the TOH effect, provided the Dirac cone remains gapless. We find that the magnitude of the response increases significantly with increasing tilt strength and warping, and therefore, they can provide the tunability of this effect. In addition, we also explore the effect of chemical doping on the TOH response in this system. Interestingly, we show, based on the symmetry analysis, that the TOH can be the leading-order response in this system, which can directly be verified in experiments.

DOI: [10.1103/PhysRevB.107.245141](https://doi.org/10.1103/PhysRevB.107.245141)

I. INTRODUCTION

In recent times topological transport has attracted immense interest since its technological applications are versatile for engineering magnetic and electrical devices [1–5]. Such topological response in the linear regime manifests in various forms, namely, the quantum Hall effect (QHE) [6], quantum spin Hall effect (QSHE) [7], quantum anomalous Hall effect (QAHE) [8,9], anomalous Nernst effect [10], and so on. The emergence of different kinds of responses strongly depends on the interplay of the topology and symmetry of the system. For instance, generating the QHE requires applying an external magnetic field, whereas, QSHE takes place in the absence of magnetic field, demanding that the system has time reversal symmetry (TRS). On the other hand, QAHE originates from the intrinsic magnetic moment present in the system which also breaks TRS. In essence, it is the geometric nature of the wave functions, also called Berry curvature (BC) [11,12], which is at the root of all such topological responses. While the normal Hall-like response originates in magnetic systems, it was shown recently that nonmagnetic systems without inversion symmetry (IS) and in the presence or absence of mirror symmetry can give rise to a higher-order Hall response, namely, the second-order nonlinear Hall effect

(NLHE) [13–20]. These responses are caused by either the BC itself or its first moment, i.e., the BC dipole of all the occupied states. Importantly, the nonlinear response is a Fermi surface dependent quantity coupled to the BC.

It is well known that in systems in which both IS and TRS are present, the BC is identically zero in magnitude. Interestingly, it was proposed very recently that such systems can, in principle, give rise to third-order Hall (TOH)-like response. This response originates from the variation of the field-induced Berry connection $\mathcal{A}^{(1)}$ with respect to an applied electric field \mathbf{E} . Even though the Berry connection itself is not a gauge-invariant quantity, $G_{ab}(\mathbf{k}) = \frac{\partial \mathcal{A}_a^{(1)}(\mathbf{k})}{\partial E_b}$, termed the Berry connection polarizability (BCP), is a gauge-invariant quantity, where a and b represent Cartesian coordinates [21–23]. Polarizability in electrodynamics indicates an affinity of matter to gain an electric dipole moment in the presence of an applied electric field. One can similarly argue that Bloch electrons acquire positional shift due to the external electric field yielding a third-order Hall effect (TOHE) [24].

Generically, there are a plethora of noncentrosymmetric Dirac and Weyl materials which have been proposed to realize a NLHE [25–42]. Most of these systems possess a large BC centered around the Dirac or Weyl nodes. Apart from searching for the NLHE in TRS-preserving but IS-breaking materials, a large class of materials which have both TRS and IS exists. For those systems, it is naturally of interest to understand higher-order Hall responses, namely,

*czeng@bit.edu.cn

†snehasish12@lanl.gov

the TOHE. Recently, experimental works reported T_d -MoTe₂ and few-layer WTe₂ flakes possess such a third-order response [43,44]. An in-plane circular photogalvanic effect in 1T'-MoTe₂, caused by a third-order nonlinear optical effect, was experimentally observed recently [45].

Motivated by the above experiments, in this work, we seek to answer the following question: How does TOHE (i.e., $\propto E^3$) show up on the surface states of a strong three-dimensional (3D) topological insulator (TI)? Using the framework of semiclassical Boltzmann transport theory, we first consider the general expression of the TOH current, mediated by BCP, which is linearly proportional to the relaxation time τ . Our study indicates that the TOH response can appear as the leading-order response in a TRS-invariant system containing a nontilted Dirac cone; this can directly be verified in experiments. The magnitude of the response is enhanced significantly by increasing the hexagonal warping strength which is inherently present in the surface states of 3D TIs. This originates from the fact that a BCP tensor acquires higher values with increasing warping. The TOHE becomes more pronounced with band tilt that breaks C_3 symmetry; however, the BCP tensor is insensitive to tilt. Moreover, we also explore the effect of chemical doping on the TOH response and discuss in detail how to separate the TOH response from linear and second-order effects in experiments using the symmetry arguments.

The rest of this paper is organized as follows. In Sec. II, we present the detailed formalism of semiclassical Boltzmann transport theory for the TOHE. Following this, in Sec. III we elucidate the TOHE in the surface states of a 3D TI in both the absence and presence of hexagonal warping. Finally, in Sec. IV we conclude by summarizing our results and discussing possible future directions.

II. SEMICLASSICAL FORMALISM OF TOHE

In this section, we present the general expression for BCP-induced TOH conductivity in the absence of external magnetic field within the framework of the Boltzmann transport formalism with the relaxation time approximation [21,24,46]. We start with the Boltzmann transport equation in its phenomenological form [47,48],

$$\left(\frac{\partial}{\partial t} + \dot{\mathbf{r}} \cdot \nabla_{\mathbf{r}} + \dot{\mathbf{k}} \cdot \nabla_{\mathbf{k}}\right) f_{\mathbf{k},\mathbf{r},t} = I_{\text{coll}}\{f_{\mathbf{k},\mathbf{r},t}\}, \quad (1)$$

where the right side, $I_{\text{coll}}\{f_{\mathbf{k},\mathbf{r},t}\}$, is known as the collision integral incorporating the effects of electron correlations and impurity scattering. The nonequilibrium electron distribution function is denoted by $f_{\mathbf{k},\mathbf{r},t}$. Now under the relaxation time approximation the steady-state Boltzmann equation reads

$$(\dot{\mathbf{r}} \cdot \nabla_{\mathbf{r}} + \dot{\mathbf{k}} \cdot \nabla_{\mathbf{k}}) f_{\mathbf{k}} = \frac{f_0 - f_{\mathbf{k}}}{\tau(\mathbf{k})}, \quad (2)$$

where $\tau(\mathbf{k})$ is the scattering time. For simplicity, we ignore the momentum dependence of $\tau(\mathbf{k})$ in all the calculations and assume it is a constant [49,50]. The equilibrium distribution function $f_0(\mathbf{k})$ in the absence of applied electric field \mathbf{E} is given by the Fermi-Dirac distribution function,

$$f_0(\mathbf{k}) = \frac{1}{1 + e^{\beta[\epsilon(\mathbf{k}) - \mu]}}, \quad (3)$$

where $\beta = 1/(k_B T)$ and $\epsilon_{\mathbf{k}}$ and μ are the energy dispersion and chemical potential, respectively.

To study the BC-induced linear Hall effect, a first-order correction of the band energy due to the orbital magnetic moment is sufficient. This is because the orbital magnetic moment couples to the applied magnetic field \mathbf{B} , giving rise to an anomalous velocity component for the electrons [12]. Conversely, systems preserving TRS can yield a second-order Hall effect with the application of a strong enough electric field. This occurs by virtue of the dipole moment of the BC, which in this case generates the anomalous velocity component [13]. However, in the case of the TOHE, one needs a second-order semiclassical theory for Bloch electrons under uniform electromagnetic fields in terms of the physical position and crystal momentum, which are fully gauge invariant. This theory includes a first- (second-) order field correction to the BC (band energy) and modifies the relation between the physical position and crystal momentum with regard to the canonical ones [46]. To be precise, being perturbed by an electric field \mathbf{E} with $H'_E = e\mathbf{E} \cdot (\mathbf{r} - \mathbf{r}_c)$, the wave packet acquires a positional shift with respect to its center \mathbf{r}_c in terms of the second-order correction in the electric field [46].

Now including n th-order field corrections of the BC $\tilde{\Omega}_{\mathbf{k}}$ and band energy $\tilde{\epsilon}_{\mathbf{k}}$, the semiclassical equations of motion in the absence of magnetic field can be written as

$$\dot{\mathbf{r}} = \frac{1}{\hbar} \nabla_{\mathbf{k}} \tilde{\epsilon}_{\mathbf{k}} - \dot{\mathbf{k}} \times \tilde{\Omega}_{\mathbf{k}}, \quad \hbar \dot{\mathbf{k}} = e\mathbf{E}, \quad (4)$$

with $e < 0$. Here, $\tilde{\epsilon}_{\mathbf{k}}$ and $\tilde{\Omega}_{\mathbf{k}}$ are given by

$$\tilde{\epsilon}_{\alpha,\mathbf{k}} = \sum_{i=0}^n \epsilon_{\alpha,\mathbf{k}}^{(i)}, \quad \tilde{\Omega}_{\alpha\delta,\mathbf{k}} = \nabla_{\mathbf{k}} \times \sum_{i=0}^n \mathbf{A}_{\alpha\delta}^{(i)}(\mathbf{k}), \quad (5)$$

where $\epsilon_{\alpha,\mathbf{k}}^{(0)}$ and $\mathbf{A}_{\alpha\delta}^{(0)}(\mathbf{k})$ are the unperturbed band energy and interband Berry connection or non-Abelian Berry connection matrix, respectively, where $\mathbf{A}_{\alpha\delta}^{(0)}(\mathbf{k})$ can be expressed as $\mathbf{A}_{\alpha\delta}^{(0)}(\mathbf{k}) = \langle u_{\alpha\mathbf{k}}^{(0)} | i \nabla_{\mathbf{k}} | u_{\delta\mathbf{k}}^{(0)} \rangle$, with $|u_{\alpha\mathbf{k}}^{(0)}\rangle$ being the cell-periodic part of the Bloch eigenstate in the unperturbed case and α and δ being band indices. In this work, we restrict ourselves to $n = 1$ and $n = 2$ for the BC and band energy, respectively.

Assuming minimal coupling and using standard perturbation theory, the first-order $\mathcal{O}(E)$ correction of the Bloch wave function can be written as

$$|u_{\alpha\mathbf{k}}^{(1)}\rangle = \sum_{\delta \neq \alpha} \frac{|u_{\delta\mathbf{k}}^{(0)}\rangle \langle u_{\delta\mathbf{k}}^{(0)} | H'_E | u_{\alpha\mathbf{k}}^{(0)} \rangle}{\epsilon_{\alpha,\mathbf{k}}^{(0)} - \epsilon_{\delta,\mathbf{k}}^{(0)}} = \sum_{\delta \neq \alpha} \frac{e\mathbf{E} \cdot \mathbf{A}_{\delta\alpha}^{(0)} | u_{\delta\mathbf{k}}^{(0)} \rangle}{\epsilon_{\alpha,\mathbf{k}}^{(0)} - \epsilon_{\delta,\mathbf{k}}^{(0)}}, \quad (6)$$

where $\mathbf{r} = i\partial_{\mathbf{k}}$ has been applied. However, the first-order correction to the band energy vanishes, i.e., $\epsilon_{\alpha}^{(1)} = \langle u_{\alpha\mathbf{k}}^{(0)} | H'_E | u_{\alpha\mathbf{k}}^{(0)} \rangle = 0$ as $\langle u_{\alpha\mathbf{k}}^{(0)} | \mathbf{r} | u_{\alpha\mathbf{k}}^{(0)} \rangle = \mathbf{r}_c$ [46]. Importantly, the first-order Berry connection, measuring a shift in its center of mass position wave packet, incorporates $\mathcal{O}(E)$, written as

$$\mathbf{A}_{\alpha,a}^{(1)} = 2\text{Re} \sum_{\delta} \frac{\mathbf{A}_{\alpha\delta,a}^{(0)} \mathbf{A}_{\delta\alpha,b}^{(0)}}{\epsilon_{\alpha,\mathbf{k}}^{(0)} - \epsilon_{\delta,\mathbf{k}}^{(0)}} E_b = G_{\alpha,ab} E_b. \quad (7)$$

Here, $\mathbf{A}_{\alpha,a}^{(1)}$ gives the positional shift of the band α , and G_{ab} is known as the BCP tensor and is a purely geometric quantity. Note that the center of mass position is given by $\mathbf{r}_{c,\alpha} = \mathbf{r}_{0,\alpha} + \mathbf{A}_{\alpha}^{(0)} + \mathbf{A}_{\alpha}^{(1)}$, where $\mathbf{r}_{0,\alpha}$ is a constant, $\mathbf{A}_{\alpha}^{(0)} \sim \mathcal{O}(E^0)$ is gauge

dependent, and $\mathbf{A}_\alpha^{(1)} \sim O(E^1)$ involves gauge-independent Berry connection polarizability. It is important to note that the zeroth-order energy can be effectively considered to be $\epsilon^{(0)} = \epsilon_k + \mathbf{E} \cdot \mathbf{r}_c$ such that the total perturbative Hamiltonian $H_E = \mathbf{E} \cdot \mathbf{r} = \mathbf{E} \cdot (\mathbf{r} - \mathbf{r}_c) + \mathbf{E} \cdot \mathbf{r}_c$. However, this additional term is k independent, acting like a potential energy, leading to an overall shift of the energy. On the other hand, in the second-order semiclassical theory, r_c and the momentum k are viewed as independent variables. Therefore, it is clear $\frac{\partial \epsilon^{(0)}}{\partial k} = \frac{\partial \epsilon_k}{\partial k}$, implying that the additional term will not play any role in our calculation [51]. Now, the second-order $O(E^2)$ correction to band energy becomes

$$\epsilon_\alpha^{(2)} = \sum_{\delta \neq \alpha} \frac{|\langle u_{\delta k}^{(0)} | H'_E | u_{\alpha k}^{(0)} \rangle|^2}{\epsilon_{\alpha, k}^{(0)} - \epsilon_{\delta, k}^{(0)}} = \frac{e^2 E_a G_{ab} E_b}{2}. \quad (8)$$

Note that $\epsilon_\alpha^{(1)}$ and $\mathbf{A}_\alpha^{(0)}$ ($\epsilon_\alpha^{(2)}$ and $\mathbf{A}_\alpha^{(1)}$) are gauge-dependent (gauge-independent) quantities.

Considering uniform electric field (i.e., $\dot{\mathbf{r}} \cdot \nabla_{\mathbf{r}} f(\mathbf{k}) = 0$), the semiclassical Boltzmann equation in Eq. (2) reads

$$\dot{\mathbf{k}} \cdot \nabla_{\mathbf{k}} f_k = \tau^{-1} (f_0 - f_k). \quad (9)$$

$$\begin{aligned} \mathbf{j}_3 = & - \int [d\mathbf{k}] (\mathbf{E} \times \Omega_k^{(0)}) [\epsilon^{(2)} f'_0(\mathbf{k})] + \tau \int [d\mathbf{k}] v_k^{(0)} (\mathbf{E} \cdot \nabla_{\mathbf{k}}) [\epsilon^{(2)} f'_0(\mathbf{k})] + \tau \int [d\mathbf{k}] v_k^{(2)} (\mathbf{E} \cdot \nabla_{\mathbf{k}}) f_0(\mathbf{k}) \\ & - \tau \int [d\mathbf{k}] (\mathbf{E} \times \Omega_k^{(1)}) (\mathbf{E} \cdot \nabla_{\mathbf{k}}) f_0(\mathbf{k}) - \tau^2 \int [d\mathbf{k}] (\mathbf{E} \times \Omega_k^{(1)}) (\mathbf{E} \cdot \nabla_{\mathbf{k}})^2 f_0(\mathbf{k}) + \tau^3 \int [d\mathbf{k}] v_k (\mathbf{E} \cdot \nabla_{\mathbf{k}})^3 f_0(\mathbf{k}), \end{aligned} \quad (11)$$

where $[d\mathbf{k}]$ is the notation for $d^d \mathbf{k} / (2\pi)^d$, with d being the dimension of the system; $f'_0(\mathbf{k}) = \frac{\partial f_0(\mathbf{k})}{\partial \epsilon_k}$; and $v_k^{(i)} = \frac{\partial \epsilon_k^{(i)}}{\partial k}$. It is clear from the above expression that all the terms contain the energy derivative of the Fermi-Dirac distribution function, and therefore, the Hall effect associated with this current is caused purely by the Fermi surface. Here, the first term is independent of the relaxation time, and this is caused by the combination of anomalous velocity, induced by the BC, and the second-order field correction of the band energy. The first term hence yields a purely intrinsic TOHE. On the other hand, the second and third terms in Eq. (11) are linearly proportional to τ , appearing due to the second-order energy correction in the distribution function and the velocity, respectively. The fourth and fifth terms arise mainly due to the anomalous velocity produced by the field-induced BC. The last term, which is proportional to τ^3 , is purely semiclassical and emerges due to band velocity.

Since in the present work we are interested in the contribution of the TOHE originating from the BCP, we will drop the semiclassical term from now on. However, we point out that one can separate this term from the others by looking at the τ scaling in experiment [33]. It is expected that the third-order current will have a very small signal compared to the first-order current in experiment. Therefore, in this work, we consider the TRS-invariant system so that BC-mediated linear anomalous Hall effect vanishes, which otherwise becomes dominant for TRS-broken systems. It is important to note that the purely intrinsic first term $\propto \tau^0$ and anomalous velocity related fourth term $\propto \tau^2$ in Eq. (11) vanish in the TRS-

One can consider the following ansatz to be the solution of the above Boltzmann equation:

$$f_k = \sum_{m=0}^{\infty} (\tau \mathbf{E} \cdot \nabla_{\mathbf{k}})^m f_0(\tilde{\epsilon}_k). \quad (10)$$

Here, we expand the solution in terms of the external electric field, which is considered to be small in the semiclassical regime. The ansatz chosen in Eq. (10) reduces to the equilibrium distribution function $f_0(\epsilon_k^{(0)})$ for $m = 0$. Note that the ansatz is usually chosen with the band velocity and energy derivative of the equilibrium Fermi function $\partial f_0 / \partial \epsilon_k^{(0)}$. In the present method of representation, the velocity $\tilde{v}_k = \frac{1}{\hbar} \frac{\partial \epsilon_k}{\partial k}$ is replaced by the momentum derivative $\nabla_{\mathbf{k}}$, while the Fermi-distribution function contains the modified energy $f_0(\tilde{\epsilon}_k)$ such that the effect of the electric field is not double counted. As already discussed, modified energy contains the electric-field-induced correction terms $\tilde{\epsilon}_k = \epsilon_k^{(0)} + \epsilon_k^{(1)} + \epsilon_k^{(2)} + \dots$.

Plugging the expression of $\dot{\mathbf{r}}$ and f_k given in Eqs. (4) and (10), respectively, into the expression of current density $\mathbf{j} = e \int [d\mathbf{k}] \dot{\mathbf{r}} f_k$ and simplifying further, one can obtain the third-order current (i.e., $\propto E^3$), which can be written as (considering $e = \hbar = 1$) [21]

invariant system. Therefore, the third-order current expression has terms only proportional to τ for a TRS-invariant system. It is also important to note that another contribution proportional to τ^2 in the nonlinear planar Hall effect can appear in TRS-broken systems arising from the combination of unperturbed BC and band energy [52–54]. In addition to the purely intrinsic term in Eq. (11), the second-order field-dependent BC arising from the second-order field-induced positional shift can generate an additional contribution to the TOH for a TRS-broken system [51]. However, the second-order field-induced Berry connection contributes only to the TOH for a TRS-broken system, in contrast to the TRS-invariant system, in which the first-order field-induced Berry connection contributes to the TOH.

It is instructive to rewrite the third-order current given by Eq. (11) in component form as

$$j_{3,a} = \chi_{abcd} E_b E_c E_d, \quad (12)$$

where the third-order conductivity tensor χ_{abcd} is a fourth-rank tensor which can generate both the longitudinal and transverse third-order current responses. Now, from Eq. (11), the third-order conductivity tensor χ_{abcd} for a TRS-invariant system can be written in terms of the BCP tensor as [21]

$$\begin{aligned} \chi_{abcd}^{(3)} = & \tau \int [d\mathbf{k}] [\partial_a \partial_b G_{cd} - \partial_a \partial_d G_{bc} + \partial_b \partial_d G_{ac}] f_0(\mathbf{k}) \\ & - \frac{\tau}{2} \int [d\mathbf{k}] v_a^{(0)} v_b^{(0)} G_{cd} f_0''(\mathbf{k}), \end{aligned} \quad (13)$$

where we use $\partial_i \partial_j = \partial_j \partial_i$, $G_{ij} = -G_{ji}$, $v_i f'_0(\mathbf{k}) = \partial_i f_0(\mathbf{k})$, and $\int [d\mathbf{k}] \partial_i G_{jk} \partial_l f_0(\mathbf{k}) = -\int [d\mathbf{k}] \partial_l G_{jk} \partial_i f_0(\mathbf{k})$. We now wish to separate the conductivity tensor into the components that contribute to the power and dissipationless Hall components. Considering the fact that the current and electric fields transform as vectors under coordinate changes, we now decompose the $\chi_{abcd}^{(3)}$ tensor into symmetric ($\chi_{abcd}^{(3),S}$) and antisymmetric ($\chi_{abcd}^{(3),A}$) parts with respect to the first two indices as $\chi_{abcd}^{(3)} = \chi_{abcd}^{(3),S} + \chi_{abcd}^{(3),A}$ [21]. Note that $\chi_{(ab)cd}^{(3),A}$ represents the dissipationless TOH conductivity tensor. In connection to Eq. (12), the BCP-induced third-order response is not constrained by TRS and IS. However, crystalline symmetries are very important for observing the TOHE. The TOHE vanishes when the two-dimensional (2D) system possesses C_{3v} , C_{6v} , D_3 , D_{3h} , D_{3d} , and D_6 symmetries, while C_3 and C_6 symmetries force the TOH current to be isotropic. Importantly, the mirror symmetry along j , M_j , constrains $\chi_{ijjj}^{(3)} = \chi_{iiij}^{(3)} = 0$, with $i \neq j$. Interestingly, the spin susceptibility of the BCP leads to a nonlinear planar Hall effect, allowed by C_n , C_{nv} , and D_n ($n = 2, 3, 4, 6$) symmetries, for the TRS-broken case [55].

It is important to note that the BC-induced first-order, second-order, and TOH responses can appear simultaneously in experiment for a system with both the TRS and IS broken. However, one can easily separate them from each other via frequency lock-in (ac) measurements, specifically, by measuring second-harmonic and third-harmonic Hall resistance [43]. In dc measurements, they can also be distinguished based on the above symmetry analysis. It has been shown that in a TRS-invariant 2D system, the presence of single mirror symmetry forces the Berry curvature dipole (BCD)-induced second-order Hall conductivity to be orthogonal to the mirror plane. On the other hand, the TOH conductivity vanishes in the direction orthogonal to the mirror plane. Therefore, this fact can isolate second-order Hall and TOH responses in a TRS-invariant but IS-broken system in which the linear Hall response already vanishes due to the presence of TRS.

Based on the above symmetry analysis, we now make remarks on real systems in which the BCP-induced TOH response will be the dominant one. Unlike the first- and second-order Hall effects, the third-order response is not restricted by TRS and IS. The TOHE appears to be the leading one in nonmagnetic centrosymmetric materials in which both first- and second-order responses are forced to vanish. Apart from nonmagnetic centrosymmetric systems, it is also possible to have the TOHE be the leading one in noncentrosymmetric systems. For example, in two dimensions, the BCD-induced second-order response can be suppressed due to the presence of a twofold (screw) rotation along the z axis, and therefore, the third-order response will be the dominant one in this case. Materials having C_{3v} point group symmetries can also show the TOHE as the dominant one despite the absence of an inversion center.

III. RESULTS

In this section, we investigate the BCP-induced Hall conductivity in a two-dimensional surface Hamiltonian of a 3D topological system, specifically, in the surface states of a 3D strong TI.

We consider the two-dimensional surface Hamiltonian of a TRS-invariant strong TI (e.g., Bi_2Te_3) hosting a unique Fermi surface that encloses an odd number of Dirac cones in the surface Brillouin zone. In this system, the linear k -dependent spin-orbit coupling leads to the band inversion at the Γ point in the Brillouin zone. In addition, it contains a hexagonal warping term ($\propto k^3$) which can be understood to be a counterpart of cubic Dresselhaus spin-orbit coupling.

The reasons for choosing this system to study the TOHE are the following: (i) The linear anomalous Hall effect vanishes due to the presence of TR symmetry, (ii) the BCD-induced second-order Hall response is zero in the absence of a tilt parameter due to crystalline symmetry, (iii) this system allows us to investigate the nontrivial effects of hexagonal warping on the TOHE, and (iv) our predicted results for the TOHE can directly be checked in experiments.

Considering the threefold rotation C_3 around the z axis and mirror symmetry $M_x: x \rightarrow -x$, the low-energy model around the gapless Γ point is given by

$$H^{\text{HW}}(\mathbf{k}) = E_0(\mathbf{k}) + v_x k_x \sigma_y - v_y k_y \sigma_x + \frac{\lambda}{2}(k_+^3 + k_-^3) \sigma_z, \quad (14)$$

where $E_0(k) = \frac{k^2}{2m^*}$ causes the particle-hole asymmetry, which for simplicity is ignored here. Here, v_x and v_y are the Dirac velocities along the x and y directions, respectively, which we consider to be k independent without loss of generality; $k_{\pm} = k_x \pm ik_y$, and λ is the strength of hexagonal warping.

Now the energy dispersion of the above Hamiltonian becomes

$$E^{\pm}(\mathbf{k}) = \pm \sqrt{v^2 k^2 + \lambda^2 k^6 \cos \phi}, \quad (15)$$

where $\phi = \arctan(\frac{k_y}{k_x})$ and $+$ ($-$) represents the conduction (valence) band. The band dispersion has sixfold symmetry under $\phi \rightarrow \phi + \frac{2\pi}{6}$. In the absence of warping, it is clear from Eq. (15) that the Fermi surface, obtained from $f'_0(\mathbf{k})$, is circular. After turning on the hexagonal warping term, the Fermi surface remains circular for small warping strength. With increasing warping strength, the shape of the Fermi surface becomes noncircular with relatively sharp tips extending along a high-symmetry direction and curves inward in between, leading to a snowflakelike structure [56]. Note that the surface states depicted by the Hamiltonian given in Eq. (14) preserve TR symmetry.

Interestingly, the in-plane surface magnetic field, realized by in-plane magnetization doping or the proximity effect of ferromagnetic insulators with in-plane magnetization, does not gap out the surface Dirac cones. However, the position of the Dirac points in the Brillouin zone changes under such in-plane magnetic field, causing the anisotropic spin texture [57,58]. Such anisotropy can be effectively considered through a tilt term under certain conditions. In addition, the electric field can also lead to surface inversion symmetry as well as particle-hole symmetry breaking, which can be modeled by the additional tilt term where the effect of the in-plane magnetic field can also be absorbed [59]. The arbitrary termination of the TI can also lead to the breaking of particle-hole symmetry in the surface states [57,58].

Under such conditions, we can consider a generic surface Hamiltonian in the presence of a tilt term $\omega k_x \sigma_0$. Here,

ω is the tilt strength along the k_x direction. In addition, the C_3 symmetry breaking can naturally bring perturbation terms to the Hamiltonian in Eq. (14). Among these the leading contribution can be effectively described by the above tilted term. Such a band tilt term was recently shown to play an important role in studies of transport phenomena [60–62]. In this work, we discuss its effects on the TOHE. It is important to note that our analysis is also applicable for the crystalline topological insulator in which there exists an effective TRS symmetry by which one tilted Dirac cone gets mapped to other tilted cones under the TRS operation.

In order to calculate the third-order conductivity, we first compute the different components of the BCP tensor. One can analytically find the following components:

$$\begin{aligned} G_{xx} &= 4[k_y^2 v_x^2 v_y^2 + 4k_x^6 v_x^2 \lambda^2 + 9k_y^2 v_y^2 \lambda^2 (k_x^2 + k_y^2)]/d^3, \\ G_{yy} &= 4k_x^2 [(k_x^2 + 3k_y^2)^2 v_y^2 \lambda^2 + v_x^2 (v_y^2 + 36k_x^2 k_y^2 \lambda^2)]/d^3, \\ G_{yx} &= -4[3k_x^5 k_y (4v_x^2 + v_y^2) \lambda^2 + 6k_x^3 k_y^3 v_y^2 \lambda^2 \\ &\quad + k_x k_y v_x^2 v_y^2 - 9k_x^5 v_y^2 \lambda^2]/d^3, \end{aligned} \quad (16)$$

where $d = [k_x^2 v_x^2 + k_y^2 v_y^2 + k_x^2 \lambda^2 (k_x^2 - 3k_y^2)^2]^{1/2}$. The distributions of the xx , yy , and xy components are depicted in the top, middle, and bottom rows of Fig. 1 for warping strength $\lambda = 0.05\lambda_0$, $0.40\lambda_0$, and $1.0\lambda_0$, respectively. The Fermi surface of the system for warping strength $\lambda = 250 \text{ eV } \text{\AA}^3$ and band tilt $w = 0, 0.2v_x$ is shown in the bottom row of Fig. 1. It is clear from the insets in Fig. 1 that near the Γ point, the diagonal components of the BCP show a dipolelike structure [dipole along y (x) for G_{xx} (G_{yy})], whereas the off-diagonal component (G_{xy}) exhibits a quadrupolelike structure for a particular strength of λ . Interestingly, although the diagonal components do not change sign, the off-diagonal components shows a sign change with π periodicity. This can be well understood from the approximated analytical form of the BCP components for $\lambda \rightarrow 0$,

$$\begin{aligned} G_{xx} &\simeq 4k_y^2 v_x^2 v_y^2 / (k_x^2 v_x^2 + k_y^2 v_y^2)^{3/2}, \\ G_{yy} &\simeq 4k_x^2 v_x^2 v_y^2 / (k_x^2 v_x^2 + k_y^2 v_y^2)^{3/2}, \\ G_{xy} &\simeq -4k_x k_y v_x^2 v_y^2 / (k_x^2 v_x^2 + k_y^2 v_y^2)^{3/2}, \end{aligned} \quad (17)$$

where it is clear that $G_{xx} \rightarrow G_{xx}$ for $k_y \rightarrow -k_y$, $G_{yy} \rightarrow G_{yy}$ for $k_x \rightarrow -k_x$, and $G_{xy} \rightarrow -G_{xy}$ for $(k_x, k_y) \rightarrow (-k_x, k_y)$ or $(k_x, k_y) \rightarrow (k_x, -k_y)$.

Now to explore the warping effect on the BCP tensor we need to look away from the Γ point because the warping term $\propto k^3$ acquires a very small value close to the Γ point (note that this effect vanishes at the Γ point). We find that the magnitude of the BCP components increases with increasing λ away from the Γ point. In particular, G_{xx} captures the snowflakelike structure, whereas G_{yy} and G_{xy} show the sharp tips and inward curves caused by the warping effect. To be precise, G_{yy} and G_{xy} show quadrupolar features caused by the warping effect (see middle and bottom rows in Fig. 1). The four legs of the quadrupole acquire the same sign for G_{yy} , while the sign changes between two consecutive legs for G_{xy} . The quadrupolar structure can be caused by

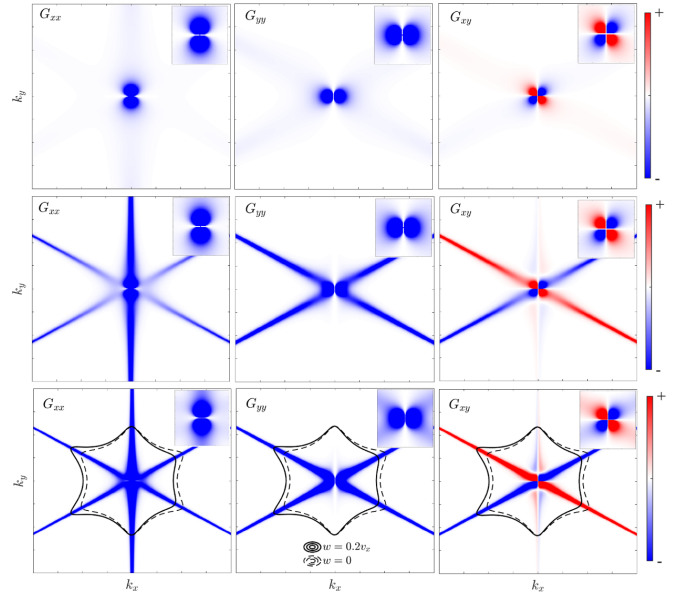


FIG. 1. BCP tensors G_{xx} (left column), G_{yy} (middle column), and G_{xy} (right column) for the Dirac cone, derived from Eq. (14), with warping strength $\lambda = 0.05\lambda_0$, $0.40\lambda_0$, and $1.0\lambda_0$ in top, middle, and bottom rows, respectively. With increasing warping strength, G_{xx} displays a snowflakelike structure, whereas G_{yy} and G_{xy} show quadrupolar features for \mathbf{k} significantly far from the Γ point. The four legs of the quadrupole acquire the same sign for G_{yy} , while the sign changes between two consecutive legs for G_{xy} . Insets show a close-up view of BCP components near the Γ point, where the diagonal components show dipolelike structure, whereas the off-diagonal component exhibits quadrupolelike structure. The tilt parameter w does not affect the BCP tensor; it results in a change in the Fermi surface, as indicated by the black lines in the bottom row for $E_f = 0.3 \text{ eV}$. We consider the following parameters, representing Bi_2Te_3 : $v_x = v_y = 2.55 \text{ eV } \text{\AA}$ and $\lambda_0 = 250 \text{ eV } \text{\AA}^3$, with the band tilt strengths w given in the panels. The color scale used for the insets is 10 times the main plot's color scale.

$k_x k_y$ -product terms in G_{yy} and G_{xy} . This nature is substantially different from the BC, which always shows a snowflakelike structure with any finite warping strength. It is important to note that the tilt parameter does not affect the BCP tensor, and it causes only the anisotropic shifting of the Fermi surface along the tilt direction. This is also depicted in the bottom row of Fig. 1. Notice that the behavior of the BCP tensor close to the Γ point remains insensitive to the warping strength, as shown in the insets in Fig. 1. This observation can be analytically understood from the expression of the BCP tensor derived above. We want to mention that the variation in the BCP magnitude and the anisotropy in the Fermi surface can either simultaneously or separately impact the net TOH responses.

With the BCP tensor in hand, we will now calculate the TOH conductivity using Eq. (12). We would like to point out that since the system is invariant under mirror symmetry M_x , the tensor components involving an odd number of x and y (e.g., χ_{xxxxy} , χ_{yyxxx}) vanish. To explore the angular dependence of the TOHE, we consider the applied electric field $\mathbf{E} = E(\cos \theta, \sin \theta, 0)$, making an angle θ with the x axis (that is, perpendicular to the mirror line in the current study).

Since we are interested in the TOH response, the transverse third-order conductivity can be written as

$$\chi_3^H(\theta) = J_3^H / E^3, \quad (18)$$

where $J_3^H = \mathbf{j}_3 \cdot (\hat{\mathbf{z}} \times \mathbf{E})$ is the current flowing perpendicular to the applied electric field. Now using the above equation, the explicit expression of $\chi_3^H(\theta)$ can be obtained as

$$\begin{aligned} \chi_3^H(\theta) = & (3\chi_{21} - \chi_{11}) \sin \theta \cos^3 \theta \\ & - (3\chi_{12} - \chi_{22}) \sin^3 \theta \cos \theta, \end{aligned} \quad (19)$$

where $\chi_{11} = \chi_{xxxx}$, $\chi_{22} = \chi_{yyyy}$, $\chi_{12} = \frac{1}{3}(\chi_{xxyy} + \chi_{xyxy} + \chi_{xyyx})$, and $\chi_{21} = \frac{1}{3}(\chi_{yyxx} + \chi_{yxyx} + \chi_{yxxxy})$. It is now clear from the expression that the TOH current vanishes along (with $\theta = \pi/2$) and perpendicular (with $\theta = 0$) to the mirror line.

In the absence of tilting, the C_3 symmetry is preserved, and the Fermi surface is circular when $v_x = v_y$. Therefore, $\chi_3^H(\theta)$ vanishes due to the symmetry constraint. Now to get the finite contribution of the TOHE, one needs to break the C_3 symmetry. This can be achieved by introducing the tilt parameter ω where the Dirac cone remains gapless. Alternatively, one can consider anisotropic Dirac velocities, i.e., $v_x \neq v_y$, preserving TRS, to break C_3 symmetry. Note that the hexagonal warping term does not break C_3 symmetry. The variation of χ_3^H as a function of θ for different tilt strengths is shown in the top panel of Fig. 2. It is important to note that the BCP is singular at $k = 0$ for the gapless surface states of TIs, which is very similar to that of the Berry curvature and Berry curvature dipole when two bands approach each other (around the degenerate points). However, one can consider an infinitesimal constant in the gap in the numerical calculations to avoid the singularity. We find that although the qualitative changes remain the same, the magnitude of the conductivity increases with increasing tilt strength. This happens because the stronger band tilt provides a more anisotropically warped Fermi surface, which straightforwardly modifies the net contribution of the current [see Eqs. (10)–(12)]. Next, we show the variation of $\chi_3^H(\theta)$ in the middle panel of Fig. 2 for different warping strengths λ with chemical potential $\mu = 0.25$ eV and $\omega = 0.2$. Clearly, the magnitude of the TOH conductivity increases with an increase of the warping strength, which can be visualized from the evaluation of the BCP tensor with warping. Finally, we investigate the effect of doping on $\chi_3^H(\theta)$. We find that the peak positions of $\chi_3^H(\theta)$ shift toward a lower angle, whereas the dip positions shift toward a higher angle. Moreover, the response becomes very strong for $\mu > 0.2$ eV as the warping effect of the surface Dirac cone is apparent only above some chemical potential threshold [56].

It is interesting to note that for the C_3 -broken, TRS-preserved case with an anisotropic nontilted 2D Dirac cone (i.e., $v_x \neq v_y$), the BCD-induced and disorder-mediated second-order Hall conductivity vanishes. This is because such responses are proportional to the tilt factor ω associated with the identity term [13,15]. By contrast, the BCP-induced TOHE survives. Noticeably, the TOHE is not directly related to the tilt factor as the BCP tensor is insensitive to ω . Therefore, the TOH response could be the leading-order response for TI systems consisting of a nontilted anisotropic Dirac cone on the surface states because of the presence of TRS.

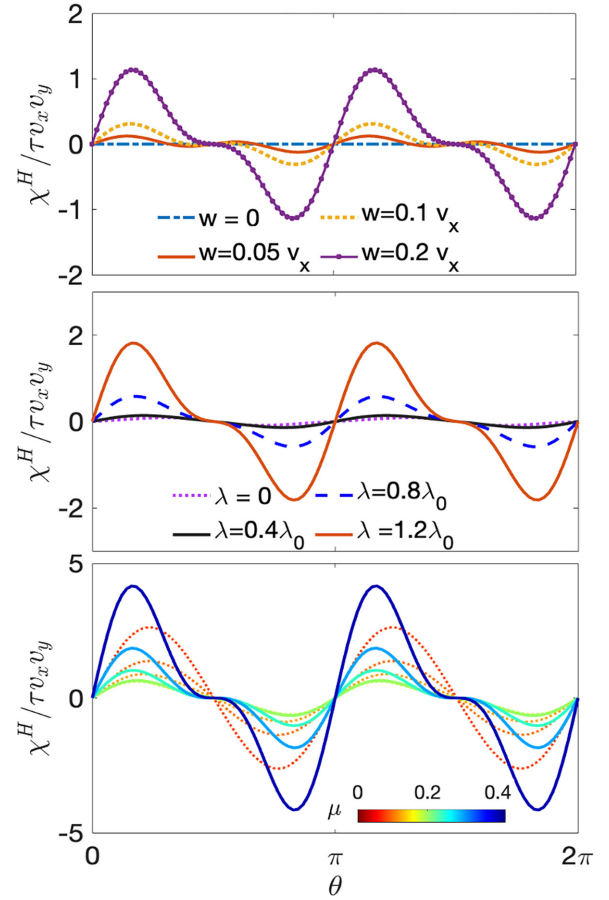


FIG. 2. TOH conductivity (scaled with $\tau v_x v_y$) for the surface states of 3D TI as a function of the angle θ between the applied electric field and x axis. The angular variation of TOH conductivity with tilt strength ω (top) for fixed $\mu = 0.25$ eV and $\lambda_0 = 250$ eV \AA^3 , warping strength λ (middle) for fixed $\mu = 0.25$ eV and $\omega/v_x = 0.2$, and chemical potential μ (bottom) for fixed $\lambda_0 = 250$ eV \AA^3 and $\omega/v_x = 0.2$ are shown. The TOH conductivity scaled with $\tau v_x v_y$ is measured in units of eV^{-3} .

IV. DISCUSSION AND CONCLUSIONS

In summary, within the framework of the quasiclassical Boltzmann theory, we considered the general expression of the TOH current. We showed that in a TRS-invariant system, the TOH current, appearing due to the BCP tensor, is proportional to relaxation time τ . Using the symmetry arguments, we established that such a BCP-induced TOH response can become the leading-order response in the surface states of 3D TIs in the absence of tilting of the Dirac cone. This provides a direct check for the TOHE in experiments.

We explored the effect of warping strength, chemical doping, and tilt on the TOH response in this system. We found that the magnitude of the TOH conductivity can be enhanced significantly by increasing the hexagonal warping strength λ which is inherently present in the surface states of 3D TIs such as Bi_2Te_3 (see Fig. 2). This is related to the fact that the magnitudes of the BCP tensor components, shown in Fig. 1, increase with increasing λ away from the Γ point. Our study also revealed that the tilt strength has no effect on the BCP tensor, unlike the warping parameter; however, the tilt parameter

can also tune the TOHE by enhancing the anisotropy of the Fermi surface. As the BCP is very dependent on the warping strength, the effective TOHE was also shown to exhibit more significant signals at the higher chemical potential where the warping becomes evident for the surface states.

We here comment on the possible experimental predictions as far as the values of the TOHE are concerned. For a 20 quintuple layer (QL) thick ($t \sim 20$ nm) TI material (e.g., Bi_2Te_3) fabricated in the conventional Hall bar geometry with size $l \times w = 100 \times 20 \mu\text{m}^2$ [52,63], considering resistivity $\rho = 700 \mu\Omega \text{ cm}$ and scattering time $\tau = 5.86 \times 10^{-13}$ s, a current drive with a magnitude of $I_0 = 0.6$ mA can provide an electric field $E = 105 \text{ V cm}^{-1}$. When the field angle θ is around $\theta \sim \pi/6$ (see the top panel of Fig. 2), the induced TOH voltage $U_H \propto \chi_3^H E^3$ at $\mu = 0.25$ eV can be estimated to be $U_H \sim 14.02 \mu\text{V}$ when a weak band tilt $w/v_x = 0.05$ is present. A moderate band tilt $w/v_x = 0.20$ can even lead to a TOH voltage on the order of $U_H \sim 0.129$ mV. Similar estimations can also be made for TI surface Dirac states when they are non-tilted but have slightly anisotropic Fermi velocities ($v_x \neq v_y$).

Moreover, we also discussed in detail how to separate the third-order Hall response from linear and second-order effects in experiments. Since the list of topological materials possessing warping and tilt at the same time is diverse, our work opens an avenue for searching for the TOHE in various

topological systems. It is important to note that the effective mass of the material can reduce the warping effect; fortunately, as demonstrated in experiments, the warping effect is, indeed, present for the surface states in TIs. Specifically, effect of the suppression coming from the effective mass on the warping effect (as well as the band tilt) is found to be much lower in Bi_2Te_3 than in other TIs [62,64–66]. Therefore, the BCP-driven nonlinear transport discussed in our work is expected to be experimentally viable for Bi_2Te_3 .

ACKNOWLEDGMENTS

The work at Los Alamos National Laboratory (LANL) was carried out under the auspices of the U.S. Department of Energy (DOE) National Nuclear Security Administration under Contract No. 89233218CNA000001. It was supported by the LANL LDRD Program and in part by the Center for Integrated Nanotechnologies, a DOE BES user facility, in partnership with the LANL Institutional Computing Program for computational resources. S.K.D. was partially supported by the Startup Grant of Bitan Roy from Lehigh University. C.Z. acknowledges support from NSFC (Grant No. 12104043), a fellowship of the China Postdoctoral Science Foundation (Grant No. 2021M690409), and the National Key R&D Program of China (Grant No. 2020YFA0308800).

-
- [1] M. Z. Hasan and C. L. Kane, *Rev. Mod. Phys.* **82**, 3045 (2010).
 - [2] M. Z. Hasan and J. E. Moore, *Annu. Rev. Condens. Matter Phys.* **2**, 55 (2011).
 - [3] X.-L. Qi and S.-C. Zhang, *Rev. Mod. Phys.* **83**, 1057 (2011).
 - [4] D. Pesin and A. H. MacDonald, *Nat. Mater.* **11**, 409 (2012).
 - [5] Y. Ando, *J. Phys. Soc. Jpn.* **82**, 102001 (2013).
 - [6] K. v. Klitzing, G. Dorda, and M. Pepper, *Phys. Rev. Lett.* **45**, 494 (1980).
 - [7] C. L. Kane and E. J. Mele, *Phys. Rev. Lett.* **95**, 226801 (2005).
 - [8] F. D. M. Haldane, *Phys. Rev. Lett.* **61**, 2015 (1988).
 - [9] C.-X. Liu, S.-C. Zhang, and X.-L. Qi, *Annu. Rev. Condens. Matter Phys.* **7**, 301 (2016).
 - [10] D. Xiao, Y. Yao, Z. Fang, and Q. Niu, *Phys. Rev. Lett.* **97**, 026603 (2006).
 - [11] M. V. Berry, *Proc. R. Soc. London, Ser. A* **392**, 45 (1984).
 - [12] D. Xiao, M.-C. Chang, and Q. Niu, *Rev. Mod. Phys.* **82**, 1959 (2010).
 - [13] I. Sodemann and L. Fu, *Phys. Rev. Lett.* **115**, 216806 (2015).
 - [14] S. S. Samal, S. Nandy, and K. Saha, *Phys. Rev. B* **103**, L201202 (2021).
 - [15] S. Nandy and I. Sodemann, *Phys. Rev. B* **100**, 195117 (2019).
 - [16] O. Matsyshyn and I. Sodemann, *Phys. Rev. Lett.* **123**, 246602 (2019).
 - [17] S. K. Das, T. Nag, and S. Nandy, *Phys. Rev. B* **104**, 115420 (2021).
 - [18] T. Nag and D. M. Kennes, *Phys. Rev. B* **105**, 214307 (2022).
 - [19] B. Sadhukhan and T. Nag, *Phys. Rev. B* **104**, 245122 (2021).
 - [20] B. Sadhukhan and T. Nag, *Phys. Rev. B* **103**, 144308 (2021).
 - [21] H. Liu, J. Zhao, Y.-X. Huang, X. Feng, C. Xiao, W. Wu, S. Lai, W. Gao, and S. A. Yang, *Phys. Rev. B* **105**, 045118 (2022).
 - [22] M. Wei, L. Xiang, L. Wang, F. Xu, and J. Wang, *Phys. Rev. B* **106**, 035307 (2022).
 - [23] Z.-F. Zhang, Z.-G. Zhu, and G. Su, [arXiv:2209.08556](https://arxiv.org/abs/2209.08556).
 - [24] Y. Gao, S. A. Yang, and Q. Niu, *Phys. Rev. B* **91**, 214405 (2015).
 - [25] T. Low, Y. Jiang, and F. Guinea, *Phys. Rev. B* **92**, 235447 (2015).
 - [26] Y. Zhang, Y. Sun, and B. Yan, *Phys. Rev. B* **97**, 041101(R) (2018).
 - [27] C. Zeng, S. Nandy, and S. Tewari, *Phys. Rev. B* **103**, 245119 (2021).
 - [28] J. I. Facio, D. Efremov, K. Koepf, J.-S. You, I. Sodemann, and J. van den Brink, *Phys. Rev. Lett.* **121**, 246403 (2018).
 - [29] Z. Z. Du, C. M. Wang, H.-Z. Lu, and X. C. Xie, *Phys. Rev. Lett.* **121**, 266601 (2018).
 - [30] J.-S. You, S. Fang, S.-Y. Xu, E. Kaxiras, and T. Low, *Phys. Rev. B* **98**, 121109(R) (2018).
 - [31] Q. Ma *et al.*, *Nature (London)* **565**, 337 (2019).
 - [32] Y. Zhang, J. van den Brink, C. Felser, and B. Yan, *2D Mater.* **5**, 044001 (2018).
 - [33] Z. Z. Du, C. M. Wang, S. Li, H.-Z. Lu, and X. C. Xie, *Nat. Commun.* **10**, 3047 (2019).
 - [34] E. J. König, M. Dzero, A. Levchenko, and D. A. Pesin, *Phys. Rev. B* **99**, 155404 (2019).
 - [35] K. Kang, T. Li, E. Sohn, J. Shan, and K. F. Mak, *Nat. Mater.* **18**, 324 (2019).
 - [36] J. Son, K.-H. Kim, Y. H. Ahn, H.-W. Lee, and J. Lee, *Phys. Rev. Lett.* **123**, 036806 (2019).
 - [37] R. Battilomo, N. Scopigno, and C. Ortix, *Phys. Rev. Lett.* **123**, 196403 (2019).
 - [38] C. Zeng, S. Nandy, A. Taraphder, and S. Tewari, *Phys. Rev. B* **100**, 245102 (2019).
 - [39] X.-Q. Yu, Z.-G. Zhu, J.-S. You, T. Low, and G. Su, *Phys. Rev. B* **99**, 201410(R) (2019).

- [40] D. Kumar, C.-H. Hsu, R. Sharma, T.-R. Chang, P. Yu, J. Wang, G. Eda, G. Liang, and H. Yang, *Nat. Nanotechnol.* **16**, 421 (2021).
- [41] C. Ortix, *Adv. Quantum Technol.* **4**, 2100056 (2021).
- [42] Z. Z. Du, C. M. Wang, H.-P. Sun, H.-Z. Lu, and X. C. Xie, *Nat. Commun.* **12**, 5038 (2021).
- [43] S. Lai, H. Liu, Z. Zhang, J. Zhao, X. Feng, N. Wang, C. Tang, Y. Liu, K. S. Novoselov, S. A. Yang, and W. bo Gao, *Nat. Nanotechnol.* **16**, 869 (2021).
- [44] X.-G. Ye, P.-F. Zhu, W.-Z. Xu, Z. Zang, Y. Ye, and Z.-M. Liao, *Phys. Rev. B* **106**, 045414 (2022).
- [45] J. Ma, R. A. Muniz, S. Qi, J. Lai, K. Zhang, Y. Liu, X. Zhuo, S. Chen, J.-H. Chen, S. Zhou, and D. Sun, *2D Mater.* **8**, 025016 (2021).
- [46] Y. Gao, S. A. Yang, and Q. Niu, *Phys. Rev. Lett.* **112**, 166601 (2014).
- [47] N. W. Ashcroft and N. D. Mermin, *Solid State Physics* (Holt, Rinehart and Winston, New York, 1976).
- [48] J. M. Ziman, *Electrons and Phonons: The Theory of Transport Phenomena in Solids* (Oxford University Press, Oxford, 2001).
- [49] S. Nandy, G. Sharma, A. Taraphder, and S. Tewari, *Phys. Rev. Lett.* **119**, 176804 (2017).
- [50] T. Nag and S. Nandy, *J. Phys.: Condens. Matter* **33**, 075504 (2021).
- [51] L. Xiang, C. Zhang, L. Wang, and J. Wang, *Phys. Rev. B* **107**, 075411 (2023).
- [52] P. He, S. S.-L. Zhang, D. Zhu, S. Shi, O. G. Heinonen, G. Vignale, and H. Yang, *Phys. Rev. Lett.* **123**, 016801(R) (2019).
- [53] W. Rao, Y.-L. Zhou, Y.-J. Wu, H.-J. Duan, M.-X. Deng, and R.-Q. Wang, *Phys. Rev. B* **103**, 155415 (2021).
- [54] R. Battilomo, N. Scopigno, and C. Ortix, *Phys. Rev. Res.* **3**, L012006 (2021).
- [55] Y.-X. Huang, X. Feng, H. Wang, C. Xiao, and S. A. Yang, *Phys. Rev. Lett.* **130**, 126303 (2023).
- [56] L. Fu, *Phys. Rev. Lett.* **103**, 266801 (2009).
- [57] F. Zhang, C. L. Kane, and E. J. Mele, *Phys. Rev. B* **86**, 081303(R) (2012).
- [58] F. Zhang, C. L. Kane, and E. J. Mele, *Phys. Rev. Lett.* **110**, 046404 (2013).
- [59] P. Somroob, T. Sutthibutpong, S. Tangwanchaoen, and W. Liewrian, *Phys. E (Amsterdam, Neth.)* **127**, 114501 (2021).
- [60] S.-H. Zheng, H.-J. Duan, J.-K. Wang, J.-Y. Li, M.-X. Deng, and R.-Q. Wang, *Phys. Rev. B* **101**, 041408(R) (2020).
- [61] S.-B. Zhang, C.-A. Li, F. Peña-Benitez, P. Surówka, R. Moessner, L. W. Molenkamp, and B. Trauzettel, *Phys. Rev. Lett.* **127**, 076601 (2021).
- [62] C. Zeng, X.-Q. Yu, Z.-M. Yu, and Y. Yao, *Phys. Rev. B* **106**, L081121 (2022).
- [63] P. He, S. S.-L. Zhang, D. Zhu, Y. Liu, Y. Wang, J. Yu, G. Vignale, and H. Yang, *Nat. Phys.* **14**, 495 (2018).
- [64] Z. Alpichshev, J. G. Analytis, J.-H. Chu, I. R. Fisher, Y. L. Chen, Z. X. Shen, A. Fang, and A. Kapitulnik, *Phys. Rev. Lett.* **104**, 016401 (2010).
- [65] M. Nomura, S. Souma, A. Takayama, T. Sato, T. Takahashi, K. Eto, K. Segawa, and Y. Ando, *Phys. Rev. B* **89**, 045134 (2014).
- [66] E. Annese, T. Okuda, E. F. Schwier, H. Iwasawa, K. Shimada, M. Natamane, M. Taniguchi, I. P. Rusinov, S. V. Eremeev, K. A. Kokh, V. A. Golyashov, O. E. Tereshchenko, E. V. Chulkov, and A. Kimura, *Phys. Rev. B* **97**, 205113 (2018).